Accepted Manuscript

The efficient long-term inhibition of forsterite dissolution by common soil bacteria and fungi at earth surface conditions

Eric H. Oelkers, Liane G. Benning, Stefanie Lutz, Vasileios Mavromatis, Christopher R. Pearce, Oliver Plümper

Please cite this article as: Oelkers, E.H., Benning, L.G., Lutz, S., Mavromatis, V., Pearce, C.R., Plümper, O., The efficient long-term inhibition of forsterite dissolution by common soil bacteria and fungi at earth surface conditions, *Geochimica et Cosmochimica Acta* (2015), doi: http://dx.doi.org/10.1016/j.gca.2015.06.004

THE EFFICIENT LONG-TERM INHIBITION OF FORSTERITE DISSOLUTION BY COMMON SOIL BACTERIA AND FUNGI AT EARTH SURFACE CONDITIONS

Eric H. Oelkers[1,2,**], Liane G. Benning[3,4], Stefanie Lutz[3], Vasileios Mavromatis[1,5], Christopher R. Pearce[6], and Oliver Plümper[7]

[1]Geoscience and Environment Toulouse (GET), CNRS, UMR 5563, Observatoire Midi-Pyrénées, 14 Avenue Edouard Belin, 31400 Toulouse, France

[2]Earth Sciences, University College London, Gower Street, London WC1E 6DT, United Kingdom

[3]School of Earth and Environment, The University of Leeds, Leeds LS2 9JT,United Kingdom

[4]GFZ German Research Centre for Geosciences, Telegrafenberg, D-14473 Potsdam, Germany

[5]Institute of Applied Geosciences, Graz University of Technology, Rechbauerstrasse 12, A-8010 Graz, Austria

[6]National Oceanography Centre, University of Southampton Waterfront Campus, European Way, Southampton, SO14 3ZH, United Kingdom

[7]Department of Earth Sciences, Utrecht University, P.O. Box 80.021, 3508 Utrecht, The Netherlands

Abstract – San Carlos forsterite was dissolved in initially pure H_2O in a batch reactor in contact with the atmosphere for five years. The reactive fluid aqueous pH remained relatively stable at pH 6.7 throughout the experiment. Aqueous Mg concentration maximized after approximately two years time at 3×10^{-5} mol/kg, whereas aqueous Si concentrations increased continuously with time, reaching 2×10^{-5} mol/kg after 5 years. Element release rates closely matched those determined on this same forsterite sample during short-term abiotic open system experiments for the first 10 days, then slowed substantially such that the Mg and Si release rates are approximately an order of magnitude slower than that calculated from the short-term abiotic experiments. Post-experiment analysis reveals that secondary hematite, a substantial biotic community, and minor amorphous silica formed on the dissolving forsterite during the experiment. The biotic community included bacteria, dominated by *Rhizobiales (Alphaproteobacteria)*, and fungi, dominated by *Trichocomaceae*, that grew in a carbon and nutrient-limited media on the dissolving forsterite. The Mg isotope composition of the reactive fluid was near constant after 2 years but 0.25‰ heavier in $\delta^{26}Mg$ than the dissolving

---

[*]CORRESPONDING AUTHOR: E-mail: oelkers@get.obs-mip.fr ; Telephone: +33 5.61.33.25.75

forsterite. Together these results suggest long-term forsterite dissolution in natural Earth surface systems maybe substantially slower that estimated from short-term abiotic experiments due to the growth of biotic communities on their surfaces.

1. INTRODUCTION

The goal of this study was to improve our understanding of forsterite reactivity in natural Earth surface systems. Towards this goal, forsteritic olivine was dissolved in initially pure H_2O in a batch reactor for 5 years. Although no carbon or nutrients were added to the reactor, a community of microbes developed on the dissolving forsterite during the experiment. The temporal evolution of the reactive fluid chemistry and post-experiment analysis of the solid phases, including DNA sequencing, were used to provide insight into microbial-mineral interaction and to assess the degree to which this microbial community affected forsterite reactivity. Magnesium isotopic analyses were performed to determine how microbially mediated forsterite dissolution fractionates this element between the solid and fluid phase. The purpose of this communication is to report the results of this experimental study, providing insight into both the ability to harvest divalent metal cations from forsterite for mineral carbonation, and how microbial communities may affect weathering rates over extended time frames at Earth surface conditions.

The reactivity of forsterite and its silicate alteration products has received increasing attention as a potential source material for the divalent cations required to carbonate CO_2 during carbon storage efforts (e.g. Giammar et al., 2005; Oelkers and Schott, 2005; Bearat et al., 2006; Matter et al., 2007; Oelkers et al., 2008; Dufaud et al., 2009; Prigiobbe et al., 2009; Matter and Kelemen, 2009; King et al., 2010; Beinlich et al, 2012; Daval et al., 2011; Guyot et al., 2011; Broecker, 2012; Kohler et al., 2013; Gislason and Oelkers, 2014; Sissmann et al., 2014). This interest has led to a large number of studies aimed at characterizing forsterite dissolution behavior and rates at various fluid compositions and temperatures (Luce et al., 1972; Sanemasa et al., 1972, Grandstaff, 1978, 1986, Murphy and Helgeson, 1987, 1989; Blum and Lasaga, 1988, Banfield et al., 1990; Wogelius and Walther, 1991, 1992; Casey and Westrich, 1992, Awad et al., 2000, Chen and Brantley, 2000, Rosso and Rimstidt, 2000, Pokrovsky and Schott, 2000a, 2000b, Oelkers, 2001b, Giammar et al., 2005, Hänchen et al., 2006, Olsen and Rimstidt, 2008; Davis et al., 2009; Beinlich and Austrheim, 2012; Rimstidt et al., 2012; Olsson et al., 2012; Plümper et al., 2012; Wang and Giammar, 2012; Garcia et al., 2013; Saldi et al., 2013; van Noort et al., 2013; Bundeleva et al., 2014; Delcercq et al., 2014; Johnson et al., 2014; King et al., 2011, 2014; Martinez et al., 2014; Torres et al., 2014).

A large fraction of these forsterite dissolution experiments were performed at acidic conditions, either due to the presence of aqueous HCl (e.g. Casey and Westrich, 1992; Oelkers, 2001b) or at elevated CO_2 pressures (e.g. Saldi et al., 2013; Wang and Giammar, 2013; Johnson et al., 2014). More significantly, the bulk of these experiments were performed over short time periods; for example Olsen and Rimstidt (2008) reported forsterite dissolution rates based on experiments performed for a total of only two hours each.

A number of studies, however, suggest that the long-term dissolution behavior of dissolving olivine may be significantly different from its initial short-term behavior. Mg was observed to be preferentially released relative to Si from the forsterite surface during the initial stages of its dissolution at acidic pH (Seyama et al., 1996; Pokrovsky and Schott, 2000a, 2000b; Zakaznova-Herzog et al. 2008; Oelkers et al., 2009; King et al., 2011). This behavior can result in the formation of a Si-enriched surface layer that may polymerize and influence dissolution rates; Daval et al. (2011) reported that forsterite dissolution rates decrease as acidic CO_2-rich fluids become saturated with respect to amorphous silica, similar to the behavior previously observed for multi-component mineral and glass dissolution (e.g. Grambow, 1985; Grambow and Muller, 2001; Oelkers, 2001a). Alternatively, the surface topography of the mineral itself can evolve due to dissolution altering its average reactivity (e.g. Bandsrra and Brantley, 2008; Luttge et al., 2013). In addition, the dissolving olivine surface can become covered by secondary minerals and/or bacteria (c.f. Giammar et al., 2005; Zakaznova-Herzog et al. 2008; Olssen et al., 2012; Wang and Giammar, 2012; Hövelmann et al., 2013; Saldi et al., 2013). The degree to which secondary surface precipitates affect the dissolution rates of the primary mineral appears to depend on the structural match between the two minerals and the presence of interconnected porous pathways in the secondary phases (Hodson, 2003; Cubillas et al., 2005; Putnis, 2009; Stockmann, 2011, 2013; Saldi et al., 2013). Finally, long-term olivine dissolution rates can also be limited by the slow precipitation rates of secondary minerals, which could lead the fluid to approach equilibrium with the dissolving mineral (e.g. Zhu and Lu, 2009; Zhu et al., 2010; Saldi et al., 2012). This study was motivated in part to assess how these various processes might influence forsterite dissolution rates over time-scales larger than those typically considered in laboratory studies.

A number of studies demonstrated that processes such as secondary mineral formation, adsorption and/or uptake by higher plants occurring during weathering may alter the Mg isotopic composition of residual fluids (e.g. Black et al., 2008; Bolou-Bi et al., 2010; Li et al., 2010; Wimpenny et al., 2010; Opfergelt et al., 2012, 2014; Pogge von Strandmann et al.,

2008; Shirokova et al., 2013; Teng et al., 2010; Tipper et al., 2010; Hwang et al., 2012; Ilina et al., 2103; Mavromatis et al., 2012, 2014). Such processes could lead to global riverine fluxes that are isotopically lighter in Mg compared to the homogenous chondritic composition of the Earth's mantle (Tipper et al., 2006). Conversely, the formation of secondary carbonate minerals is known to preferentially remove isotopically light Mg isotopes from solution, causing the residual liquid to have a heavier composition (Mavromatis et al., 2014; Beinlich et al., 2014). Consequently isotopic analysis of the experimental solutions may help to quantify whether Mg isotope fractionation occurs during forsterite dissolution, and what impact this may have on the composition of fluids at the Earth's surface.

2. MATERIALS AND METHODS

2.1 Batch reactor experiment

This study reports on the result of a single 5-year forsterite dissolution experiment performed in a batch reactor system. The San Carlos forsterite sample used in this study was originally prepared by Pokrovsky and Schott (2000a and b), who reported that its composition is consistent with $Mg_{1.82}Fe_{0.18}SiO_4$ (Fo_{91}). San Carlos Olivine has been reported to contain numerous trace elements including ~40 ppm P (De Hoog et al., 2010). Transparent crystals 0.5 cm in size were handpicked, ground with an agate mortar and pestle, and sieved. The size fraction between 50 and 100 μm was ultrasonically cleaned using alcohol to remove fine particles and dried overnight at 60°C. X-ray diffraction analysis of this material shows it to be pure forsterite free of clay minerals and secondary phases. The specific surface area of the cleaned powder was 800 ± 20 cm^2/g as determined by Kr adsorption using the multi-point B.E.T. method. These solids were stored in a capped plastic bottle for 7 years prior to being used in this study. Samples were not further cleaned or sterilized prior to use in the experiments.

In an attempt to mimic the behaviour of grains interacting with rainwater at the Earth's surface, 0.514 g of ground forsterite was placed together with 985 g of pure demineralized H_2O in a 1 litre polypropylene reactor and closed with a non-air tight screw cap and left in a room with ambient light. The reactor was shaken by hand at monthly intervals and a total of 32 fluid samples were collected and through 0.45 μm filters using a polypropylene syringe. A list of sampling times and masses are provided in the electronic supplement. No additional filtering was performed on the sampled fluids before chemical

analysis. Shaking and sampling allowed the fluid to have regular contact with the atmosphere. The pH of the reactive fluid samples was measured using a combination glass electrode calibrated on the activity scale with NIST buffers (pH = 4.002, 6.865, and 9.180 at 25°C). Aqueous magnesium concentrations were determined by flame atomic absorption spectrophotometry using a Perkin Elmer 5100 PC spectrometer equipped with an AS-90 autosampler, with an uncertainty of ±2%. Aqueous silica concentrations were determined using the molybdate blue colorimetric method (Govett, 1961) using a Technicon analyzer with an uncertainty of ±3%. Aqueous Fe concentrations are not reported; these concentrations were generally below the 50 ppb detection limit of the furnace atomic absorption spectrometer.

In an attempt to mimic natural processes, no attempt was made to sterilize the reactor, reactive fluid, or the mineral powder prior the experiment. Similarly, toxic salts such as sodium azide (NaN_3) were not added to the reactor to prevent microbe growth. Finally, neither organic compounds nor nutrients were added to the rector, such that if a microbial community were to grow it would be required to persist on nutrients provided by the dissolving mineral and gases dissolved from the atmosphere.

2.2 Mg isotope measurements

Selected fluid samples were analyzed to determine their Mg isotopic compositions following the method described in Pearce et al. (2012) and Mavromatis et al. (2013, 2014). Typically 5–10 μg of Mg was processed for each fluid sample, and ~10 mg of forsterite was dissolved in concentrated aqueous HCl, for the solid. Each sample was evaporated until dry then dissolved in concentrated aqueous HNO_3 prior to analysis. The samples were then passed through AG50W-X12 cation exchange resin before being isotopically analysed using a Thermo-Finnigan 'Neptune' MC-ICP-MS at the Géosciences Environement Toulouse laboratory. Solution concentrations of 300 ppb typically gave beam intensities of ~4V for ^{24}Mg, with total procedural blanks having a negligible contribution of generally <10 mV. Isotopic compositions were determined via sample-standard bracketing, and are reported as $\delta^{26/24}Mg$ with respect to the DSM-3 standard (Galy et al., 2003). All samples were analysed in triplicate, with the mean value being presented. The long-term reproducibility of isotopic analyses, assessed by repeat analyses of the DSM-3 Mg standard, gave a $\delta^{26/24}Mg$ 2 standard deviation (2 σ) of 0.04 ‰.

2.3 Reacted mineral analysis

The reacted olivine powders were investigated using scanning electron microscopy (SEM) and transmission electron microscopy (TEM). Secondary electron (SE) imaging and energy-dispersive X-ray (EDX) analysis of powder samples were performed in a FEI Nova 600 NanoLab focused ion beam (FIB-)SEM. To investigate the organic/olivine interface we applied a protective Pt-coating across areas of interest that were subsequently excavated using focused Ga-ion beam milling. For TEM analysis, reacted powders were either applied via dispersion onto holey-carbon copper discs or electron transparent FIB lamellae were prepared from individual powder grains. TEM samples were characterized in a FEI Tecnai 20F operating at 200 kV, equipped with a high-angle annular dark field (HAADF) detector and an EDX system. All electron microscope analyses were executed at the Electron Microscopy Center at Utrecht University.

Raman spectra of organics covering the powder surfaces were collected using a Horiba Jobin Yvon XploRA confocal Raman spectrometer operating with the 532 nm line of a Nd:YAG laser at the Institut für Mineralogie, University of Münster, Germany. The scattered Raman light was collected in a 180° backscattering geometry and dispersed by a 1200 grooves/mm grating after passing through a 100 µm entrance slit. The spectrometer was calibrated using the first order Raman band of silica at 520.7 cm^{-1}. Observed Raman spectra were compared against the RRUFF project database (Downs, 2006) and Raman databases for microorganisms (Maquelin et al. 2002; Huang et al. 2010, and references therein).

2.4 Microrganism identification

The microorganisms that grew during the long-term forsterite dissolution experiment were identified though characterization of their ribosomal DNA. Such identification was essential in this study as no microbial communities or nutrients were added to the reactor. Total DNA was extracted using a MoBio Laboratories PowerSoil® DNA Isolation kit. 16S rRNA genes were amplified using the bacterial primers 27F (5'-AGAGTTTGATCMTGGCTCAG) and 357R (5'-CTGCTGCCTYCCGTA), tagged with the Ion Torrent adapter sequences and MID barcodes, spanning the V1-V2 hypervariable regions. 18S rRNA genes were amplified using the eukaryotic primers 528F (5′-GCGGTAATTCCAGCTCCAA) and 706R (5'-AATCCRAGAATTTCACCTCT) (Cheung et al., 2010), tagged with the Ion Torrent adapter sequences and MID barcodes, spanning the V4-V5 hypervariable region. Polymerase chain reaction (PCR) amplifications were

performed using a Platinum® PCR SuperMix, High Fidelity, according to the manufacturer's (Life Technologies) protocols. Initial denaturation at 95 ºC for 5 minutes was followed by 30 cycles of 30 seconds of denaturation at 95 ºC, annealing at 60 ºC for 30 seconds, and elongation at 72 ºC for 30 seconds. Final elongation was done at 72 ºC for 7 minutes. PCR amplifications were carried out in triplicate to reduce amplification bias in reaction volumes of 1 x 25 µl and 2 x 12.5 µl. PCR product quality and size were determined by Agarose gel electrophoreses. The pooled amplicons were cleaned with Agencourt© AMPure XP beads, with a bead to DNA ratio of 0.6 and analysed on the Agilent Technologies Agilent 2100 Bioanalyser with an Agilent Technologies High Sensitivity DNA kit to determine the quality, size, and concentration. Following these steps the 16S and 18S amplicons were sequenced on an Ion Torrent Personal Genome Machine using the Ion Xpress™ Template Kit and an Ion 314™ chip following manufacturer's protocols. The Ion Torrent sequencing was performed at the Aberystwyth Institute of Biological, Environnemental and Rural Sciences. The v4-v5 region of the 18S rRNA genes were also sequenced a second time commercially using an Illumina MiSeq sequencer at Source BioScience (UK).

The Internal Transcribed Spacer (ITS) regions of the eukaryotic ribosomal DNA (rDNA) were amplified using the primers ITS1 (5'–TCCGTAGGTGAACCTGCGG) and ITS2 (5'-GCTGCGTTCTTCATCGATGC). These PCR amplifications were performed using a Platinum® PCR SuperMix, High Fidelity, according to the manufacturer's Life Technologies protocols. Initial denaturation at 95 ºC for 5 minutes was followed by 30 cycles of 30 seconds of denaturation at 95 ºC, annealing at 55 ºC for 30 seconds, and elongation at 72 ºC for 60 seconds. The final elongation was done at 72 ºC for 7 minutes. A library was created from the cleaned PCR product and sequenced on the Illumina MiSeq (2x 250 bp) at the UK National Health Service Sheffield Diagnostic Genetics Service Centre.

Sequence processing and analyses were carried out in Qiime (Caporaso et al., 2010). Barcodes and adapter sequences were removed from each sequence. Filtering of sequences was performed using an average cutoff of Q20 over a 350 bp range. Reads shorter than 200 bp were removed. Operational taxonomic units (OTUs) were picked *de novo* using a threshold of 97% identity. Taxonomic identities were assigned for representative sequences of each OTU using Greengenes as the reference database (DeSantis et al., 2006) for 16S rRNA sequences and UNITE for ITS sequences (Kõljalg et al., 2013) and aligned using PyNAST and a 0.80 confidence threshold. Singletons were excluded from the analysis.

2.5 Geochemical modeling calculations

The chemical evolution of the long-term forsterite dissolution experiment performed in this study was modeled using the PHREEQC geochemical modeling code together with its llnl database (Parkhurst and Appello, 1999). The fluid phase was assumed to be in equilibrium with respect to the atmosphere, such that its oxidation state and dissolved inorganic carbon concentration were fixed by the atmospheric O_2 and CO_2 content. Model calculations took account of the measured forsterite surface area and fluid-solid ratio of the experiment; the surface area was assumed to be constant during the calculations. Forsterite dissolution rates were calculated using equations and parameters provided by Pokrovsky and Schott (2000b), which had been generated from abiotic open-system experiments performed using the same olivine powder and in the same laboratory as the present study. All secondary phases other than quartz were allowed to precipitate at local equilibrium with respect to the fluid phase in the model calculations. The potential effect of the presence or actions of microbes during our experiment was not accounted for in the model calculations.

3. RESULTS

The chemical evolution of the long-term forsterite dissolution experiment determined from the geochemical model is illustrated in Fig. 1. Forsterite is calculated to dissolve continuously during the model calculation, provoking the precipitation of hematite almost immediately and talc approximately 2 years (6×10^7 s) after the beginning of the experiment. The modelled concentration of aqueous Mg increases monotonically with time, whereas that of aqueous Si maximizes in concentration at the onset of talc precipitation. The aqueous Mg/Si ratio is calculated to be 1.82, corresponding to their stoichiometric release from the forsterite, during the first 6×10^7 s of the experiment; this ratio increases substantially with time after the onset of talc precipitation because the Mg/Si ratio is lower in talc than in the dissolving forsterite. The fluid pH is calculated to increase continuously during the experiment from 5.7, the pH of pure water in equilibrium with atmospheric CO_2, to 8.1 after 5 years. Although hematite is calculated to be the first secondary phase to precipitate during the experiment, this phase remains relatively minor due to the low Fe concentration of the dissolving forsterite. Talc is calculated to be the dominant secondary phase after ~2 years of forsterite dissolution. No other phases are calculated to be supersaturated other than quartz,

which is mildly supersaturated in the modelled reactive fluid from 5×10^7 to 10×10^7 s of elapsed time.

The observed chemical evolution of the fluid phase during the 5-year forsterite dissolution experiment is illustrated in Fig. 2. These results contrast significantly from those of the model calculation. The aqueous Mg concentration maximizes after approximately two years (7×10^7 s) at 3×10^{-5} mol/kg then decreases slowly thereafter. Aqueous Si concentrations increase continuously with time reaching 2×10^{-5} mol/kg after approximately 5 years (1.6×10^8 s). Consequently, the aqueous Mg/Si ratio decreases significantly with time during the final 3 years of the experiment. The reactive fluid pH decreases slowly with time from approximately 6.8 to 6.5, although it was not possible to measure the pH accurately in the fluid samples collected during the first 3×10^6 seconds of the experiment due to the low ionic strength of the fluid samples – pH measurements did not stabilize due to the low buffering capacity of these samples. These reactive fluid compositions are shown in an aqueous activity diagram in Fig. 3. It can be seen in this figure that the fluids are undersaturated with respect to all potentially forming secondary minerals in the MgO-SiO_2-H_2O-CO_2 system; note that talc is the most stable hydrous Mg-silicate mineral in the adopted thermodynamic database.

SEM images of the solids recovered at the end of the experiment are shown in Fig. 4. Etch pits are pervasive on the reacted forsterite surface. Many have a linearly elongated morphology (c.f. Fig 4a). These etch pits appear to be the preferred sites for an elongated growth (Fig. 4b). These growths formed along and outward from the reacted forsterite surface, forming a web-like structure on the surfaces of nearly every reacted forsterite grain (Figs 4c and 4d). An iron oxide phase, as identified by SEM- and TEM-EDX analysis, is present in minor amounts on some of the reacted forsterite grains (Fig 4e). Some minor amorphous Si was found to be present in isolated locations (Fig 4f).

The nature of the web-like growth on the reacted forsterite was further investigated by FIB-SEM cross-sectioning and TEM analysis (not shown). The location of a representative cross-sectional cut traversing this growth is shown in Fig 5a. An SEM image of the FIB-SEM cross-section, provided in Fig. 5b, shows it to be growing directly on the dissolving olivine. SEM-EDX analysis of this growth shows it to consist mainly of carbon and oxygen with minor P, S, Na, and Cl. Raman spectroscopy identifies the web-like growth to contain a combination of organic molecules typically affiliated with microbial life (e.g., Huang et al., 2010) as identified in Fig. 5c.

The identity of the organic growth on the dissolving olivine was determined by ribosomal DNA sequencing. In terms of the bacterial community, a total of 1526 sequences passed the Qiime quality pipeline corresponding to 208 operational taxonomic units, clustered at 97% sequence identity. *Proteobacteria* was found to be the most abundant phylum (90%) with *Alphaproteobacteria* (90%) being the dominant class and *Rhizobiales* (86.7%) the dominant order. *Cytophagia* was the second most abundant phylum (7.4%). Within the *Rhizobiales, Phyllobacteriaceae (26.5%) and Bradyrhizobiaceae* (13.6%) were the dominant families. A summary of the identified bacterial community is provided in Table 1.

In terms of the fungal community, PCR amplification with the 18S rRNA primers, although attempted two separate times, through two different approaches, and in two different laboratories, produced only a faint DNA band of the correct size on the Agarose gel. Unfortunately after PCR amplification, the optimisation and additional clean-ups (due to adapter dimers) needed for the 18S work, resulted in too little PCR product for sequencing. However, PCR amplification with the ITS primers and Illumina MiSeq sequencing resulted in 13,000 sequences, of which only 50 could be assigned using the UNITE database. Most sequences had likely lost their phylogenetic signal since the Illumina MiSeq library had to be prepared from the PCR product of the full ITS region and unassigned sequences had to be filtered out. The remaining sequences were all assigned to the same fungal species *Emericella nidulans,* which belongs to the family of the *Trichocomaceae*. *Trichocomaceae* are saprobe fungi, known to be adaptable to extreme environmental conditions, ubiquitous in soil, common associates of decaying plants, and play an important role in aggregation of soil (Daynes et al., 2012). Although relatively few of the fungi sequences could be identified, the likelihood that most of the fungal community is comprised of *Trichocomaceae* is supported by the similarity in morphology between the images shown in Fig. 4 with those of this fungi reported in the literature (e.g. Daynes et al., 2012).

The Mg isotopic evolution of the fluid phase during the long-term forsterite dissolution experiment is presented in Fig. 6. The $\delta^{26/24}$Mg isotope composition of the first measured reactive fluid samples are light is compared to that of the dissolving forsterite. However, the Mg isotope compositions of the subsequent reactive fluid samples are relatively constant and are ~0.25 ‰ heavier than the dissolving forsterite.

4. DISCUSSION

4.1 The long-term dissolution behavior of forsterite at Earth surface conditions.

Measured reactive fluid Si concentrations collected during the first four months of the long-term forsterite dissolution experiment are compared with corresponding model calculations based on forsterite dissolution rates generated from the short-term abiotic experiments of Pokrovsky and Schott (2000b) in Fig. 7. Note again that the rates of Pokrovsky and Schott (2000b) were chosen for this comparison because they were generated using the same ground mineral powder and the same laboratory as the long-term experiment described in this study, and in the absence of added microbes. As such they serve as an abiotic control for comparison in the present study. The close correspondence between modelled and measured Si concentrations during the first 10 days of the experiment demonstrates that the initial forsterite dissolution rates are consistent with those used in the model calculations. After approximately 10 days, the measured and modelled Si concentrations diverge suggesting a slowing of forsterite dissolution rates during our long-term experiments, such that Si and Mg release rates are approximately an order of magnitude lower than that calculated using the abiotic rates, based on a comparison between the slopes of the calculated curve and measured Si concentrations shown in Fig. 7 and similar plots made for Mg. We postulate that this inhibition of forsterite dissolution is due to the formation and growth of the bacterial and fungal community identified on the dissolving forsterite at the end of the experiment. This possibility is supported by the results of Garcia et al. (2013) who reported that *Escherichia Coli*, a common freshwater *Proteobacterium*, slowed the dissolution of forsterite compared to abiotic control experiments by a factor of ~2 to 3 during 7 day-long experiments.

The observed slowing of element release from forsterite may be representative of Earth surface weathering environments for a number of reasons. First, this batch reactor study was performed in initially pure water open to the atmosphere rather than an aqueous buffer solution. The pH of the fluid phase in this study appears to be fixed by the combined CO_2 input from the atmosphere, microbial metabolism, and proton consumption from forsterite dissolution. Second, the microbial community that developed in the reactor was not amended with artificial nutrients or a carbon source, thus nutrients could only be derived from the trace element content of the dissolving forsterite. Third, the microbial community that grew in the reactor was not a selected specific strain, but rather a suite of microbes common to natural

Earth surface systems. The bacterial community was dominated by *Proteobacteria,* a common soil bacterium; this is, for example, the most abundant phylum in Oklahoma tall-grass prairie soil, where the most abundant class was the *Alphaproteobacteria* (Spain et al., 2009). Similarly, *Alphaproteobacteria* is reported as being predominant in the non-rhizosphere soils of the Western Ghats (Rohini-Kumar et al., 2012), and among the three most abundant bacterial groups found in four soils across a large transect of the western hemisphere (Roesch et al., 2007). Similarly, the fungal community in our reactor was dominated by *Trichocomaceae,* a typical fungal species that dominates numerous soil environments (Fraga et al., 2010 ; Daynes et al., 2012).

A significant observation made in this study is that the microbial community grew preferentially on the active sites on the dissolving mineral surface. This is exemplified in Figs. 4a and b, where growing microbes can be seen to be present in most, if not all, of the etch pits formed on the dissolving forsterite surfaces. By preferentially colonizing actively dissolving sites, the microbes may be able to alter mineral reactivity to a far greater degree than their surface coverage might suggest. A number of studies have previously postulated that microbes preferentially attach themselves to active sites on dissolving mineral surfaces to harvest essential nutrients from the minerals (Hutchens et al., 2006; Bonneville, 2009, 2010; Balland et al., 2010). Note that the dissolving San Carlos forsterite contains a large number of the elements required for microbial growth in trace quantities (De Hoog et al., 2010).

It should be noted, however, that the concentrations of Si and Mg in the reactive fluid may underestimate the total amount of these elements released from the dissolving forsterite in our experiment. For example, the fact that the fluid phase Mg/Si ratio appears to decrease with time may be explained by the removal of Mg from the fluid. Considering the relatively small quantity of Fe precipitated during the experiment, it is likely that the main sink of this Mg released from the forsterite is its incorporation into the growing biota; Mg is the most common divalent metal in living cells having concentrations of 400-1000 mM in freshwater and marine bacteria (Fagerbakke et al., 1999; Heldal et al., 2012).

More perplexing, perhaps is the presence of minor amorphous Si at the dissolving forsterite surface at the end of the experiments, as the fluids are strongly undersaturated with respect to this phase throughout the experiment. It has nevertheless been suggested that fluids can become supersaturated locally if they are isolated from the bulk fluid leading to mineral replacement reactions (e.g. Putnis 2009; Ruiz-Agudo et al., 2012; Bray et al., 2014, 2015).

High-resolution SEM images show that the microbial community grows directly on the surface of the dissolving forsterite (see Fig. 4c and d). As amorphous Si dissolves far slower than forsterite (c.f. Marini, 2008; Schott et al., 2009) any amorphous Si precipitated at the microbial/forsterite interface would persist for substantial time after it was again exposed to the reactive fluid.

4.2 **Implications for carbon storage**

The dissolution of olivine is commonly thought to be one of the most efficient methods to obtain the divalent metal cations required for the long-term storage of CO_2 through mineral carbonation reactions (e.g. Giammar et al., 2005; Oelkers et al., 2008; Prigiobbe et al., 2009; King et al., 2010; Daval et al., 2011; Guyot et al., 2011; Gudbrandsson et al., 2012; Saldi et al., 2013). The overall rate of olivine carbonation stems from the coupling of forsterite dissolution rates with Mg-carbonate precipitation rates. Several processes can slow the dissolution rates of olivine thereby slowing the carbonation process. At elevated CO_2 pressure, such as might be encountered as part of subsurface mineral carbonation efforts, aqueous fluids will be acidic. At such conditions the formation of Si-rich protective layers may slow Mg release from olivine (e.g. Bearat et al., 2006, Deval et al., 2011; Saldi et al. 2013). An alternative to subsurface mineral carbonation is to promote olivine carbonation at the Earth's surface by distributing ground olivine onto the surfaces of farm and pasture land (Schuiling and Krijgsman, 2006; Kohler et al., 2010; Moosdorf et al., 2014), the continental coasts (Hangx and Spiers, 2009), and/or directly in the oceans (Kohler et al., 2013). At Earth surface conditions, pH is near to neutral, and the formation of Si-rich-layers at the surface of olivine is less favored (Oelkers et al., 2009). Nevertheless, the results presented in this study suggests that microbial communities may preferentially colonize the active sites on dissolving olivine surfaces, possibly to acquire the limiting nutrients they need for growth. This process can, over time, slow the release of Mg from olivine slowing substantially geo-engineered Earth surface carbon capture/storage efforts. As such, carbon drawdown from the atmosphere by the dissolution of ground olivine on the Earth's surface may be far less efficient than that predicted using dissolution rates generated from short-term abiotic olivine dissolution experiments.

4.3 **Implications for surface water Mg isotope compositions**

Our experimental results indicate that forsterite dissolution at ambient temperatures and neutral pH in the presence of a natural community of bacteria and fungi results in the

preferential release of isotopically heavy Mg. Although it was not possible to extract a pure biotic fraction and measure directly its Mg isotopic composition, it seems likely this observed fluid enrichment in heavy Mg results from the preferential uptake of light Mg by the biotic community. This possibility is supported by the observation that 1) the non-stoichiometic dissolution of forsterite observed in this study requires a Mg sink, and that 2) the microbial community is the only observed potential secondary reservoir for this Mg. Note also that [26]Mg enrichment was previously observed in cyanobacteria cultures of *Gleocapsa sp.* and *Synechococcus sp.* (Mavromatis et al., 2012; Shirokova et al., 2013).

The observation that forsterite dissolution in the presence of microbes yields a fluid that is isotopically heavy appears to contradict the occurrence of isotopically light Mg in most Earth surface fluids; the $\delta^{26/24}$Mg composition of bulk silicate Earth is -0.23 ‰, whereas the average continental runoff is -1.09 ‰ and that of modern seawater is -0.82 ‰ (Teng et al., 2007; Bourdon et al., 2010; Young and Galy, 2004; Tipper et al., 2006; Ling et al., 2011). We note that the 0.25 ‰ fractionation observed in this experiment is small relative to the ~1.2 ‰ range observed in global rivers (e.g. Tipper et al., 2006). Furthermore, the $\delta^{26/24}$Mg composition of surface waters is known to be heavily influenced by carbonate reactions; Beinlich et al. (2014) previously demonstrated that the carbonation of forsteritic olivine results in the precipitation of isotopically light Mg-carbonate minerals. Consequently the dissolution and release of isotopically light Mg from these secondary carbonates may play a more significant role in determining the $\delta^{26/24}$Mg composition of surface waters than direct Mg contribution from silicate dissolution.

5. CONCLUSIONS

The results of the 5-year forsterite dissolution experiment described above suggest that dissolution rates of Mg-silicate minerals in low temperature Earth surface environments may be substantially slowed by the growth of natural microbial communities that preferentially grow at reactive sites on their surfaces. The growth of these communities, which are generally overlooked in short-term laboratory experiments have a number of implications for chemical weathering, Earth surface carbon capture and storage efforts, and the Mg isotopic composition of Earth surface waters. Notably, the slowing of Mg release rates suggests that the weathering of ultramafic rocks and the drawdown of CO_2 by the distribution of fine-grained olivine on the Earth's surface may be far slower than that

estimated from the results of short-term abiotic laboratory experiments. The growth of the observed microbial community resulted in isotopically heavy fluid Mg isotope compositions illustrating how this process can influence natural water compositions. Taken together, these results suggest that low-temperature fluid-mineral experiments may provide a clearer representation of natural processes if they were run over longer time frames and in non-sterile conditions.

Acknowledgements

REFERENCES

Awad A., van Groos, A.F.K. and Guggenheim, S. (2000) Forsteritic olivine: Effect of crystallographic direction on dissolution kinetics. *Geochim. Cosmochim. Acta* **64**, 1765-1772.

Balland C., Poszwa A. Leyval C. and Mustin C. (2010) Dissolution rates of phyllosilicates as a function of bacterial metabolic diversity. *Geochim. Cosmochim. Acta* **74**, 5478-5493.

Bandstra, J.Z. and Brantley,S.L. (2008) Surface evolution of dissolving minerals investigated with kinetic Ising model. *Geochim. Cosmochim. Acta* **72**, 2587-2600.

Banfield J.F., Veblen D.R. and Jones B.F. (1990) Transmission electron microscopy of subsolidus oxidation and weathering of olivine. *Cont. Mineral. Petrol*. **106,** 110-123.

Bearat H., McKelvy M.J., Chizmeshya A.V.G., Gormley D., Nunez R., Carpenter R.W., Squires K., and Wolf, G.H. (2006) Carbon sequestration via aqueous olivine mineral carbonation: Role of passivating layer formation. *Envir. Sci. Tech*. **15**, 4802-4808.

Beinlich A. and Austrheim H. (2012) In situ sequestration of atmospheric CO_2 at low temperature and surface cracking of serpentinized peridotite in mine shafts. *Chem. Geol.* **332,** 32-44.

Beinlich A., Mavromatis V., Austrheim H. and Oelkers, E.H. (2014) Inter-mineral Mg isotope fractionation during hydrothermal ultramafic rock alteration – Implications for natural water compositions. *Earth. Planet. Sci. Let.* **392**, 166-176.

Beinlich A., Plümper O., Hövelmann J., Austrheim H. and Jamtveit B. (2012). Massive serpentinite carbonation at Linnajavri, N-Norway. Terra Nova **24**, 446-455.

Black J.R., Epstein E., Rains W.D., Yin Q.Z. and Casey, W.H. (2008) Magnesium-isotope fractionation during plant growth. Environ. *Sci. Tech.* **42,** 7831-7836.

Blum A.E. and Lasaga A.C. (1988) Role of surface speciation in the low-temperature dissolution of minerals. *Nature* **331,** 431–433.

Bonneville S., Smits M. M., Brown A., Harrington J., Leake J.R., Brydson R. and Benning L. G. (2009) Plant-driven fungal weathering: Early stages of mineral alteration at the nanometer scale. *Geology* **37**, 615-618.

Bonneville S., Morgan D. J., Schmalenberger A., Bray A., Brown A., Banwart S. A. and Benning L. G. (2011) Tree-mycorrhiza symbiosis accelerate mineral weathering: Evidences from nanometer-scale elemental fluxes at the hypha-mineral interface. *Geochim. Cosmochim. Acta* **75**, 6988-7005.

Bourdon B., Tipper E.T., Fitoussi C. and Stracke, A. (2010) Chondritic Mg isotope composition of the Earth. *Geochim. Cosmochim. Acta* **74,** 5069-5083

Broecker W. (2012) The carbon cycle and climate change: Memoirs of my 60 years in science. *Geochem. Perspectives* **1**, 221-340.

Bolou-Bi E.B., Poszwa A., Leyval C. and Vigier, N. (2010) Experimental determination of magnesium isotope fractionation during higher plant growth. Ge*ochim. Cosmochim. Acta* **74**, 2523-2537.

Bray A. W., Benning L. G., Bonneville S. and Oelkers E. H. (2014) Biotite surface chemistry as a function of aqueous fluid composition. *Geochim. Cosmochim. Acta* **128**, 58-70.

Bray A. W., Oelkers, E. H., Bonneville, S. Wolff-Boenisch, D. Potts, N. J., Fones G. and Benning L.G. (2015) The effect of pH, grain size and organic ligands on biotite weathering rates. *Geochim. Cosmochim. Acta.* 1**64,** 127-145.

Bundeleva I.A., Menez B., Auge T., Bodenan F., Recham N. and Guyot, F. (2014) Effect of cyanobacteria Synechoccus PCC 7942 on carbonation kinetics of olivine at 20° C *Minerals Engin.* **59,** 2-11**.**

Caporaso J. G., Kuczynski J., Stombaugh J., Bittinger K., Bushman F. D., Costello E. K., Fierer N., Pena A. G., Goodrich J. K. and Gordon, J. I. (2010) QIIME allows analysis of high-throughput community sequencing data. *Nature Methods* 7**,** 335-336.

Casey W.H. and Westrich H. (1992) Control of dissolution rates of orthosilicate minerals by divalent metal–oxygen bonds. *Nature* **355**, 157–159.

Chen Y. and Brantley S.L. (2000) Dissolution of forsteritic olivine at 65° C and 2<pH<5. *Chem. Geol.* **165,** 267-281.

Cheung M.K., Au C.H., Chu K.H., Kwan H.S., and Wong C.K. (2010) Composition and genetic diversity of picoeukaryotes in subtropical coastal waters as revealed by 454 pyrosequencing. *ISME J.* **4,** 1053-1059.

Cubillas P., Köhler S., Prieto M., Causserand C. and Oelkers E. H. (2005) How do mineral coatings affect dissolution rates? An experimental study of coupled $CaCO_3$ dissolution – $CdCO_3$ precipitation. *Geochim. Cosmochim. Acta* **69**, 5459–5476.

Daynes C.N., Zhang N., Saleeba J.A. and McGee P.A. (2012) Soil aggregates formed in vitro by saprotrophic Trichocomaceae have transient water-stability. *Soil Bio. Biochem.* **48,** 151-161.

Daval D., Sissmann O., Menguy N., Saldi G.D., Guyot F., Martinez I., Corvisier J., Garcia B.,

Machouk I., Knauss K.G., and Hellmann R. (2011) Influence of amorphous silica layer formation on the dissolution rate of olivine at 90 °C and elevated pCO$_2$. *Chem. Geol.* **284**, 193-209.

Declercq J., Bosc O., and Oelkers E.H. (2013) Do organic ligands affect forsterite dissolution? *App. Geochem.* **39,** 69-77.

De Hoog J.C.M., Gall, L., and Cornell, D.H. (2010) Trace-element geochemistry of mantle olivine and application for mantle petrognesis and geothermobarometry. *Chem. Geol*. **270,** 196-215.

DeSantis T.Z., Hugenholtz P., Larsen N., Rojas M., Brodie E.L., Keller K., Huber T., Dalevi D., Hu P. and Andersen, G.L. (2006) Greengenes, a chimera-checked 16S rRNA gene database and workbench compatible with ARB. *App. Envir. Microbiol.* **72,** 5069-5072.

Davis M.C., Brouwer W.J., Wesolowsli D.J., Anovitz L.M., Lipton A.S. and Mueller K.T. (2009) Magnesium silicate dissolution investigated by Si^{29} MAS, H^1-Si^{29} COMAS, Mg^{25} QCPMG, and H^{1}Mg^{25} CP QCPMG NMR. *Phys. Chem. Chem. Phys.* **11,** 7013-1021.

Downs, R. T. (2006) The RRUFF Project: an integrated study of the chemistry, crystallography, Raman and infrared spectroscopy of minerals. In Program and Abstract of the 19th General Meeting of the International Mineralogical Association in Kobe, Japan. O03–13.

Dufaud F., Martinez I., and Shilobreeva S. (2009) Experimental study of Mg-rich silicates carbonation at 400 and 500 °C and 1 kbar. *Chem. Geol*. **265**, 79-87.

Fagerbakke K.M., Norland, S. and Heldal M. (1999) The inorganic ion content of native aquatic bacteria. *Can. J. Microbiol.* **45,** 304-311.

Fraga, M. E., Pereria, M. G., Barbosa, D.J., Melo, M.P. (2010) Diversity of isolated Trichocomaceae from soil in two forest ecosystems. *Ciencia Florestal* **20**, 167-175.

Galy A., Yoffe, O., Janney, P.E., Williams, R.W., Cloquet, C., Alard, O., Halicz, L., Wadhwa, M., Hutcheon, I.D., Ramon, E. and Carignan, J. (2003) Magnesium isotope heterogeneity of the isotopic standard SRM980 and new reference materials for magnesium-isotope-ratio measurements. *J. Anal. At. Spectrom*. **18**, 1352-1356.

Garcia B., Lemelle L., Rose-Koga E., Perriat P., Basset R., Gillet P. and Albarede, F. (2013) An experimental model approach of biologically assisted silicate dissolution with olivine and Escherichia coli - Impact on chemical weathering of mafic and atmospheric CO$_2$ drawdown. *App. Geochem.* **31,** 216-227.

Giammar D.E., Bruant R.G. and Peters, C.A. (2005) Forsterite dissolution and magnesite precipitation at conditions relevant for deep saline aquifer storage and sequestration of carbon dioxide, *Chem. Geol.* **217**, 257-276.

Gislason S.R., and Oelkers, E.H. (2014) Carbon storage in basalt. *Science,* 344, 373-374.

Govett G.J.S. (1961) Critical factors in the colorimetric determination of silica. *Geochim. Cosmochim. Acta* **25**, 69-80.

Grambow B. (1985) A general rate equation for nuclear waste glass corrosion. *Mater, Res. Symp. Proc*. **44**, 15-27.

Grambow B. and Muller R. (2001) First-order dissolution rate law and the role of surface layers in glass performance assessment. *J. Neuc. Mat.* **298,** 112-124.

Grandstaff D.E. (1978) Changes in surface area and morphology and the mechanism of forsterite dissolution. *Geochim. Cosmochim. Acta* **42**, 1899-1901.

Grandstaff D.E. (1986) The dissolution rate of forsteritic olivine from Hawaiian beach sand. In *Rates of Chemical Weathering of Rocks and Minerals*, Colman, S.M., Dethier, D.P., Eds, Orlando, FL: Academic Press, 41-57.

Gudbrandsson S., Wolff-Boenisch D., Gislason S.R. and Oelkers E.H. (2011) An experimental study of crystalline basalt dissolution from 2 <= pH <= 11 and temperatures from 5 to 75 ºC. *Geochim. Cosmochim. Acta*, **75**, 5496-5509.

Guyot F., Daval D., Dupraz S., Martinez I., Menez B. and Sissmann, O. (2011) CO_2 geological storage: The environmental mineralogy perspective, *Comptes Rendus Geoscience*, **343,** 246-259.

Hänchen M., Prigiobbe V., Storti G., Seward T.M. and Mazotti M. (2006) Dissolution kinetics of forsteritic olivine at 90-150 ºC including effects of the presence of CO_2. *Geochim. Cosmochim. Acta* **70**, 4403-4416.

Hangx S.J. and Spiers C.J. (2009) Coastal spreading of olivine to control atmospheric CO_2 concentrations: A critical analysis of viability. *Int. J. Greenhouse Gas Cont.* **3,** 757-77.

Heldal M., Norland S., Erichsen E.S., Larsen A., Thingstand F. and Bratbak, G. (2012) Mg^{2+} as an indicator of nutritional status in marine bacteria. ISME J. 6, 2524-530.

Hodson M.E. (2003) The influence of Fe-rich coatings on the dissolution of anorthite at pH 2.6. *Geochim. Cosmochim. Acta 67*, 3355-3363.

Hövelmann J., Austrheim, H. and Jamtveit B. (2012) Microstructure and porosity evolution during experimental carbontion of a natural peridotite. *Chem., Geol*. **334,** 254-265.

Huang K.J., Teng F.Z., Wei G.J., Ma J.L. and Bao, Z.Y. (2012) Adsorption- and desorption-controlled magnesium isotope fractionation during extreme weathering of basalt in Hainan Island, China. *Earth Planet. Sci. Lett.* **359,** 73-83.

Huang W.E., Mengqiu L., Jarvis R.M., Goodrace R. and Banwart A (2010) Shining Light on the Microbial World: The Application of Raman Microspectroscopy. In Advances in Applied Microbiology (eds. A.I. Laskin, S. Sariaslani, G.M. Gadd). Academic Press, Burlington. pp. 152-186.

Hutchens E., Valsami-Jones E., Haouiya N., Chairat C., Oelkers E.H. and McEldoney S. (2006) An experimental investigation of the effect of Bacillus megaterium on apatite dissolution. *Geomicrobiol. J.* **23,** 177-182.

Ilina S.M., Viers J., Lapitsky S.A., Mialle S., Mavromatis V., Chmeleff J., Brunet P., Alekhin Y.V., Isnard H. and Pokrovsky, O.S. (2013) Stable (Cu, Mg) and radiogenic (Sr, Nd) isotope fractionation in colloids of boreal organic-rich waters. *Chem. Geol.* **342,** 63-75.

Johnson N.C., Burt T., Maher K., Rosenbauer R.J., Bird D. and Brown, G.E. (2014) Olivine dissolution and carbonation under conditions relevant for in-situ carbon storage. *Chem. Geol.* **373,** 93-105.

King H.E., Plümper O. and Putnis, A. (2010) Effect of secondary phase formation on the carbonation of olivine. *Envir. Sci. Tech.* **44,** 6503-6509.

King H.E., Plümper O., Geisler T. and Putnis A. (2011) Experimental investigation into the silification of olivine : Implications for the reaction mechanism and acid neutralization. *Am. Min.* **96,** 1503-1511.

King H.E., Satoh H., Tsukamoto, K. and Putnis A. (2014) Surface-specific measurments of olivine dissolution by phase-shift interferometry. *Am. Min.* **99,** 377-386.

Kohler P., Abrams J.F., Voelker C., Hauck J. and Wolf-Gladrow, D.A. (2013) Geoengineering impact of open ocean dissolution of olivine on atmospheric CO_2, surface ocean pH, and marine biology. *Env. Res. Let.* **8,** 014009.

Kohler P., Hartmann J., Wolf-Gladrow D.A. (2010) Geoengineering potential of artifically enhanced silicate weathering of olivine. *P.N.A.S.* **107,** 20228-20233.

Kõljalg U., Nilsson R.H., Abarenkov K., Tedersoo L., Taylor A.F.S., Bahram M,. Bates S.T., Bruns T.D., Bengtsson-Palme J., Callaghan T.M., Douglas B., Drenkhan T., Eberhardt U., Dueñas M., Grebenc T, Griffith G.W., Hartmann M., Kirk P.M., Kohout P., Larsson E., Lindahl B.D.,

Lücking R,. Martín M.P., Matheny P.B., Nguyen N.H., Niskanen T., Oja J., Peay K.G., Peintner U., Peterson M., Põldmaa K., Saag L., Saar I., Schüßler A., Scott J.A., Senés C., Smith M.E., Suija A ., Taylor D.L., Telleria M.T., Weiß M., Larsson K-H. (2013) Towards a unified paradigm for sequence-based identification of Fungi. *Moleculr Ecology* **22,** 5271-5277.

Li W.Y., Teng F.Z., Ke S., Rudnick R.L., Gao S., Wu F.Y. and Chappell B.W. (2010) Heterogeneous magnesium isotopic composition of the upper continental crust. *Geochim. Cosmochim. Acta* **74,** 6867-6884.

Ling M.X., Sedaghatpour F., Teng F.Z., Hays P.D., Strauss J. and Sun W.D. (2011) Homogeneous magnesium isotopic composition of seawater: An excellent geostandard for Mg isotope analysis. *Rapid Communications in Mass Spectrometry* **25,** 2828-2836.

Luce R.W., Bartlett R.W. and Parks, G.A. (1972) Dissolution kinetics of magnesium silicates. *Geochim. Cosmochim. Acta* **36**, 35–50

Luttge, A., Arvidson, R.S., and Fisher, C. (2013) A stochastic treatment of crystal dissolution kinetics. *Elements,* **9,** 183-188.

Maquelin K., Kirschner C., Choo-Smith L.-P., van den Braak N., Endtz H. Ph., Naumann D. and Puppels G.J. (2002) Identification of medically relevant microorganisms by vibrational spectroscopy. *J. Microbiological Methods* **51**, 255-271.

Marini L. (2006) Geological Sequestration of Carbon Dioxide: Thermodynamics, Kinetics, and Reaction Path Modeling. Elsevier, Amsterdam, 470 pp.

Martinez R.E., Weber S. and Bucher K. (2014) Quantifying the kinetics of olivine dissolution in partially closed batch reactor systems. *Chem. Geol*. **367,** 1-12.

Matter J.M., Kelemen P.B. (2009) Permanent storage of carbon dioxide in geological reservoirs by mineral carbonation. *Nat. Geosci,* **2,** 837-842.

Matter J.M., Takahashi T. and Goldberg, D. (2007) Experimental evaluation of in-situ CO_2-water-rock reactions during CO_2 injection in basaltic rocks: Implications for geological CO_2 sequestration. *Geochem. Geophys, Geosyst.,* **8**.

Mavromatis V., Gautier Q., Bosc O., Schott J. (2013) Kinetics of Mg partition and Mg stable isotope fractionation during its incorporation in calcite. *Geochim. Cosmochim. Acta* **114,** 188-203.

Mavromatis V., Pearce C.R., Shirokova L.S., Bundeleva I.A., Pokrovsky O.S., Benezeth P. and Oelkers E. H. (2012) Magnesium isotope fractionation during hydrous magnesium carbonate precipitation with and without cyanobacteria. *Geochim. Cosmochim. Acta* **76,** 161-174.

Mavromatis V., Prokushkin A.S., Pokrovsky O.S., Viers J., Korets M.A. (2014) Magnesium isotopes in permafrost-dominated Central Siberian larch forest watersheds. *Geochim. Cosmochim. Acta* **147,** 76-89.

Moosdorf N., Renforth P. and Hartmann J. (2014) Carbon dioxide effiiently of terrestial enhanced weathering. *Env. Sci.Tech*. **48,** 4809-4816.

Murphy W.M. and Helgeson H.C. (1987) Thermodynamic and kinetic constraints on reaction rates among minerals and aqueous solutions. III. Activated complexes and the pH-dependence of the rates of feldspar, pyroxene, wollastonite, and olivine hydrolysis. *Geochim. Cosmochim. Acta* **51**, 3137–3153.

Murphy, W.M. and Helgeson, H.C. (1989) Thermodynamic and kinetic constraints on reaction rates among minerals and aqueous solutions. IV. Retrieval of rate constants and activation parameters for the hydrolysis of pyroxene, wollastonite, olivine, analusite and quartz. *Am. J. Sci.* **288**, 17–101.

Oelkers E.H. (2001a) General kinetic description of multioxide silicate mineral and glass dissolution. *Geochim. Cosmochim. Acta* **65,** 3703-3719.

Oelkers E.H. (2001b) An experimental study of forsterite dissolution rate as a function of temperature and aqueous Mg and Si concentration. *Chem. Geol.* **148**, 485-494.

Oelkers E.H., Gislason S.R. and Matter J. (2008) Mineral carbonation of CO_2. *Elements* **4**, 333-337.

Oelkers E.H., Golubev S.V., Chairat C., Pokrovsky O.S. and Schott J. (2009) The surface chemistry of multi-oxide silicates. *Geochim. Cosmochim. Acta* **73**, 4617-4634.

Oelkers E.H. and Schott J. (2005) Geochemical aspects of CO_2 sequestration. *Chem. Geol.* **217**, 183-186.

Olsen A.A. and Rimstidt, D. (2008) Oxalate promoted forsterite dissolution at low pH. *Geochim. Cosmochim. Acta* **72**, 1758-1766.

Olsson J., Bovet N., Makovicky E., Bechgaard K., Balogh Z. and Stipp S.L.S. (2012) Olivine reactivity with CO_2 and H_2O on a microscale: Implications for carbon sequestration. *Geochim. Cosmochim. Acta* **77**, 86-97.

Opfergelt S., Georg R.B., Delvaux B., Cabidoche Y.M., Burton K.W. and Halliday A.N. (2012) Mechanisms of magnesium isotope fractionation in volcanic soil weathering sequences, Guadeloupe. *Earth Planet. Sci. Lett.* **341,** 176-185.

Opfergelt S., Burton K.W., Georg R.B., West A.J., Guicharnaud R.A., Sigfusson B., Siebert C., Gislason S.R. and Halliday A.N. (2014) Magnesium retention on the soil exchange complex controlling Mg isotope variations in soils, soil solutions and vegetation in volcanic soils, Iceland. *Geochim. Cosmochim. Acta* **125,** 110-130.

Parkhurst D.L. and Appelo C.A.J. (1999) User's guide to PHREEQC (version 2) — A computer program for speciation, batch-reaction, one-dimensional transport, and inverse geochemical calculations. Washington, DC: U.S. Geological Survey Water-Resources Investigations Report 99-4259, 312 p.

Pearce C.R., Saldi G.D., Schott J. and Oelkers E.H. (2012) Isotopic fractionation during congruent dissolution, precipitation and at equilibrium. Evidence from Mg isotopes. *Geochim. Cosmochim. Acta*, **92,** 170-183.

Plümper O., Royne A., Magraso A. and Jamtveit, B. (2012) The interface-scale mechanism of reaction-induced fracturing during serpentinzation. *Geology*, **40,** 1103-1106.

Pogge von Strandmann P.A.E., Burton K.W., James R.H., van Calsteren P., Gislason, S.R. and Sigfusson B. (2008) The influence of weathering processes on riverine magnesium isotopes in a basaltic terrain. *Earth Planet. Sci. Lett.* **276,** 187-197.

Pokrovsky O.S. and Schott J. (2000a) Forsterite surface composition in aqueous solutions: a combined potentiometric, electrokinetic, and spectroscopic approach. *Geochim. Cosmochim. Acta* **64**, 3299-3312.

Pokrovsky O.S. and Schott J. (2000b) Kinetics and mechanism of forsterite dissolution at 25ºC and pH from 1 to 12. *Geochim. Cosmochim. Acta* **64**, 3313-3325.

Putnis, A. (2009) Mineral replacement reactions. *Rev. Min. Geochem.* **70,** 87-124.

Prigiobbe V., Costa G., Baciocchi R., Hänchen M. and Mazzotti, M. (2009) The effect of CO_2 and salinity on olivine dissolution kinetics at 120°C. *Chem. Eng. Sci.* **64**, 3510-3515.

Rimstidt J.D., Brantley S.L. and Olsen A.A. (2012) Systematic review of forsterite dissolution rate data. *Geochim. Cosmochim. Acta* **99**, 159-178.

Roesch, L. F., W., Fulthorpe, R.R., Riva, A., Casella, G., Hadwin, A.K.M., Kent, A.D., Daroub, S.H., Camargo, F.A.O., Farmerie, W.G., Triplett, E.W. (2007) Pyrosequencing enumerates and contrasts soil microbial diversity. *ISME Journal* **1,** 283-290.

Rohini-Kumar, M., Osborne, J.W., Saravanan, V.S. (2012) Comparison of soil bacterial communities of *Pinus patula* of Nilgiris, Western Ghats with other biogeographical distinct pine forest clone

libraries. *Micobial Ecology* **66,** 132-144.

Rosso J.J. and Rimstidt J.D. (2000) A high resolution study of forsterite dissolution rates. *Geochim. Cosmochim. Acta* **64**, 797-811.

Ruiz-Agudo E., Putnis C.V., Rodriguez-Navarro C. and Putnis A. (2012) Mechanism of leached layer formation during chemical weathering of silicate minerals. *Geology,* **40,** 947-950.

Saldi G.D., Daval D., Morvan G. and Knauss K.G. (2013) The role of Fe and redox conditions in olivine carbonation rates: An experimental study of the rate limiting reactions at 90 and 150° C in open and closed systems. *Geochim. Cosmochim. Acta* **118**, 157-183.

Saldi G.D., Schott J., Pokrovsky O.S., Gautier Q. and Oelkers E.H. (2012) An experimental study of magnesite precipitation rates at neutral to alkaline conditions and 100-200° C as a function of pH, aqueous solution composition and chemical affinity. *Geochim. Cosmochim. Acta* **83**, 93-109.

Sanemasa I., Yoshida L., and Ozawa T. (1972) The dissolution of olivine in aqueous solutions of inorganic acids. *Bull. Chem. Soc. Jpn.* **45**, 1741–1746.

Schuiling R.D. and Krijgsman P. (2006) Enhanced weathering: An effective and cheap tool to sequester CO_2. *Climatic Change* **74,** 349-354.

Schott J., Pokrovsky O.S. and Oelkers E.H. (2009) The link between mineral dissolution/precipitation kinetics and solution chemistry. *Rev. Mineral. Geochem.* **70,** 207-258.

Seyama H., Soma M. and Tanaka A. (1996) Surface characterization of acid-leached olivines by X-ray photoelectron spectroscopy. *Chem. Geol.,* **129,** 209-216,

Shirokova L.S., Mavromatis V., Bundeleva I.A., Pokrovsky O.S., Benezeth P., Gerard E., Pearce C.R. and Oelkers E.H. (2013) Using Mg isotopes to trace cyanobacterially mediated magnesium carbonate precipitation in alkaline lakes. *Aquat. Geochem.* **19,** 1-24.

Sissmann O., Brunet F., Martinez I., Guyot F., Verlaguet A., Pinquier Y. and Deval D. (2014) Enhanced oliving carbonation within a basalt as compared to single-phase experiments: Reevaluating the potntial of CO_2 mineral sequestration. *Envir. Sci. Tech.,* **48,** 5512-5519.

Spain, A.M., Krumkolz, L.R., and Elshahed, M.S., 2009. Abundance, composition, diversity and novelty of soil *Proteobacteria* ISME J. 3, 992-2000.

Stockmann G.J., Wolff-Boenisch D., Gislason S.R. and Oelkers E.H. (2011) Do carbonate precipitates affect dissolution kinetics? 1: Basaltic glass. *Chem. Geol.* **284**, 306-316.

Stockmann G.J., Wolff-Boenisch D., Gislason S.R. and Oelkers E.H. (2013) Do carbonate precipitates affect dissolution kinetics? 2: Diopside. *Chem. Geol.* **337,** 56-66.

Teng F.-Z., Wadhwa M. and Helz R.T. (2007) Investigation of magnesium isotope fractionation during basalt differentiation. Implications for a chondritic composition of the terrestrial mantle. *Earth Planet. Sci. Lett.* **261**, 84-92.

Teng F.Z., Li W.Y., Rudnick R.L. and Gardner, L.R. (2010) Contrasting lithium and magnesium isotope fractionation during continental weathering. *Earth Planet. Sci. Lett.* **300,** 63-71.

Tipper E.T., Gaillardet J., Louvat P., Capmas F. and White A.F. (2010) Mg isotope constraints on soil pore-fluid chemistry: Evidence from Santa Cruz, California. *Geochim. Cosmochim. Acta* **74,** 3883-3896.

Tipper E.T., Galy A., Gaillardet J., Bickle M.J., Elderfield H. and Carder E.A. (2006) The magnesium isotope budget of the moden ocean: Constraints from riverine magnesium isotope ratios. *Earth Planet. Sci. Lett.* **250,** 241-253.

Torres, M.A. West, A.J. and Nealson, K. (2014) Microbial acceleration of olivine dissolution viasiderophore production. *Proc. Earth Planet. Sci.,* **10,** 118-122.

Van Noort R., Spiers C.J., Drury M.R., Kadianis M.T. (2013) Peridote dissolution and carbonation rates at fracture surfaces under condtions relevant for in-situ mineralizaion of CO_2. *Geochim. Cosmochim. Acta* **106,** 1-24.

Wang, F. and Giammar, D.E. (2012) Forsterite dissoltuion in saline water at elevated temperature and high CO_2 pressure. *Envir. Sci Tech.* **41,** 168-173,

Wimpenny J., Gislason S.R., James R.H., Gannoun A., Pogge Von Strandmann P.A.E. and Burton, K.W. (2010) The behaviour of Li and Mg isotopes during primary phase dissolution and secondary mineral formation in basalt. *Geochim. Cosmochim. Acta* **74**, 5259-5279.

Wogelius R.A. and Walther, J.V. (1991) Olivine dissolution at 25 ºC: effects of pH, CO_2 and organic acids. *Geochim. Cosmochim. Acta* **55**, 943-954.

Wogelius, R.A. and Walther, J.V. (1992) Olivine dissolution kinetics at the near-surface conditions. *Chem. Geol.* **97**, 101-112.

Young E.D. and Galy A. (2004) The isotope geochemistry and cosmochemistry of magnesium. Geochemistry of Non-Traditional Stable Isotopes. *Rev. Min. Geochem.* **55**, 197-230.

Zakaznova-Herzog V.P., Nesbitt H.W., Bancroft G.M. and Tse J.S. (2008) Characterization of leached layers on olivine and pyroxenes using high-resolution XPS and density functional calculations. *Geochim. Cosmochim. Acta* **72**, 69-86.

Zhu C. and Lu P. (2009) Alkali feldspar dissolution and secondary mineral precipitation in batch systems: 3. Saturation states of product minerals and reaction paths. *Geochim. Cosmochim. Acta* **73,** 3171-3200.

Zhu C., Lu P., Zheng Z. and Ganor J. (2010) Coupled alkali feldspar dissolution and secondary mineral precipitation in batch systems: 4. Numerical modeling of kinetic reaction paths. *Geochim. Cosmochim. Acta* **74,** 3963-3983.

Table 1. Percentage of bacterial OTUs recovered from the surfaces of the forsterite collected at the end of the 5-year dissolution experiment described in this study as generated using a 16S rRNA gene sequence identity of ≥97% using the Greengenes database.

Taxon	
Acidobacteria; Acidobacteriia; Acidobacteriales; Acidobacteriaceae	0.3
Actinobacteria; Actinobacteria; Actinomycetales; Microbacteriaceae	1.1
Actinobacteria; Actinobacteria; Actinomycetales; Pseudonocardiaceae; Pseudonocardia	1.3
Bacteroidetes; Cytophagia; Cytophagales; Cytophagaceae; Spirosoma	7.4
Proteobacteria; Alphaproteobacteria; Rhizobiales	46.3
Proteobacteria; Alphaproteobacteria; Rhizobiales; Bradyrhizobiaceae	12.4
Proteobacteria; Alphaproteobacteria; Rhizobiales; Bradyrhizobiaceae; Bradyrhizobium	1.3
Proteobacteria; Alphaproteobacteria; Rhizobiales; Methylobacteriaceae; Methylobacterium	0.3
Proteobacteria; Alphaproteobacteria; Rhizobiales; Phyllobacteriaceae	18.5
Proteobacteria; Alphaproteobacteria; Rhizobiales; Phyllobacteriaceae; Mesorhizobium	8.1
Proteobacteria; Alphaproteobacteria; Rhodospirillales; Rhodospirillaceae	0.4
Proteobacteria; Alphaproteobacteria; Sphingomonadales; Sphingomonadaceae	0.3
Proteobacteria; Alphaproteobacteria; Sphingomonadales; Sphingomonadaceae; Sphingomonas	2.6

Figure Captions

Figure 1. Temporal evolution of the closed system dissolution of Fo_{90} olivine as calculated using the PHREEQC computer code together with its llnl database (Parkhurst and Appelo, 1999). Calculations were performed using the olivine surface areas and reactive fluid to solid ratio of the long-term experiment performed in this study. The reactive fluid is assumed to be in equilibrium with the atmosphere containing $10^{-3.2}$ mole fraction CO_2 and 0.2 mole fraction O_2. (a) Calculated temporal evolution of reactive fluid Mg and Si concentration; (b) Calculated temporal evolution of reactive fluid pH; (c) Calculated volumes of reactants dissolved or precipitated – negative volume changes refer to dissolution, positive changes refer to precipitation.

Figure 2. Temporal evolution of the reactive fluid composition during the long-term dissolution of Fo_{90} olivine into pure H_2O in contact with the atmosphere during the experiment described in this study: (a) temporal evolution of reactive fluid Mg and Si concentration. The filled diamonds and circles represent measured reactive fluid Si and Mg concentrations, respectively, whereas the open circles correspond to Mg concentrations calculated from the corresponding Si concentration assuming stoichiometric dissolution; (b) temporal evolution of the reactive fluid pH; (c) temporal evolution of reaction fluid Mg/Si concentration ratio.

Figure 3. Logarithmic activity diagram in the system $MgO\text{-}SiO_2\text{-}H_2O\text{-}CO_2$. The open symbols represent the measured reactive fluid compositions during the long-term olivine dissolution experiment and the lines correspond to the equilibrium compositions of the indicated minerals. In this figure, fluids plotting to the left and below the equilibrium composition lines are undersaturated with respect to the minerals. The figure was created from measured fluid concentrations together with the PHREEQC computer code and its llnl database (Parkhurst and Appelo, 1999).

Figure 4. SEM images of reacted San Carlos olivine (Fo_{90}). (a) The olivine surface displaying etch pits formed by reactive fluid-mineral reactions; (b) Enlargements of the etch pits shown in (a). Arrows point at newly formed secondary phases that have apparently nucleated within the etch pits; (c) and (d) olivine surfaces showing the presence of a web-like organic growth structure (confirmed by Raman spectroscopy and DNA analysis) growing in and out from etch pits, (e) image showing the location of an iron oxide precipitate growing on the edges of dissolving olivine; (f) image showing the presence of a Si-rich secondary phase.

Figure 5. a) SEM image showing the location of a FIB-SEM cross-section traversing the organic growth on the surface of a reacted forsterite grain. b) SE image of cross section, orientated perpendicular to the surface, showing the spatial relation between the dissolving forsterite and the organic growth. c) Raman spectra of the San Carlos olivine and the organic growth. Vibrational modes of the organic growth were identified by comparison to published databases (Maquelin et al., 2002; Huang et al., 2010). The Raman spectrum of the organic growth was processed using a Savitzky-Golay smoothing algorithm. Grey area denotes those vibrations characteristic for olivine.

Figure 6. Temporal evolution of the reactive fluid Mg concentration and isotope composition (reported as $^{26/24}$Mg relative to the DSM3 standard). The filled circles designate measured fluid $^{26/24}$Mg compositions, and the corresponding error bars indicate the uncertainty (2 s.d.) of the measurement. The grey bar designates the Mg isotope composition of the dissolving forsterite. The filled squares indicate changes in fluid Mg concentration, as shown in Fig. 2.

Figure 7. Comparison of measured reactive fluid compositions with those calculated using PHREEQC together with dissolution rates reported by Pokrovsky and Schott (2000b) generated from short-term experiments performed using the same forsterite powder as in the present study (see caption of Fig. 1 for details of this model calculation). The symbols represent reactive fluid compositions measured in this study whereas the curve corresponds to model calculation results.
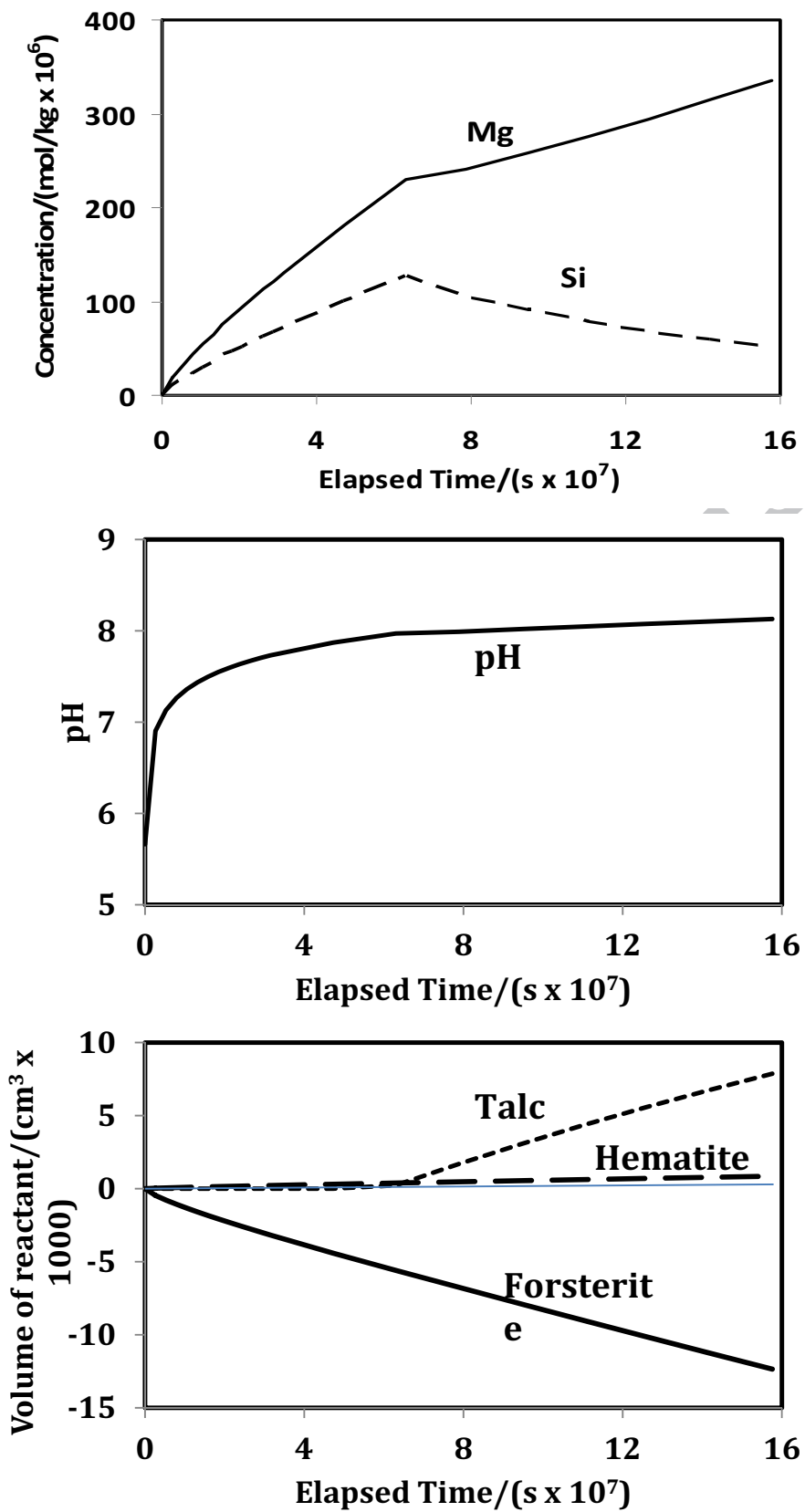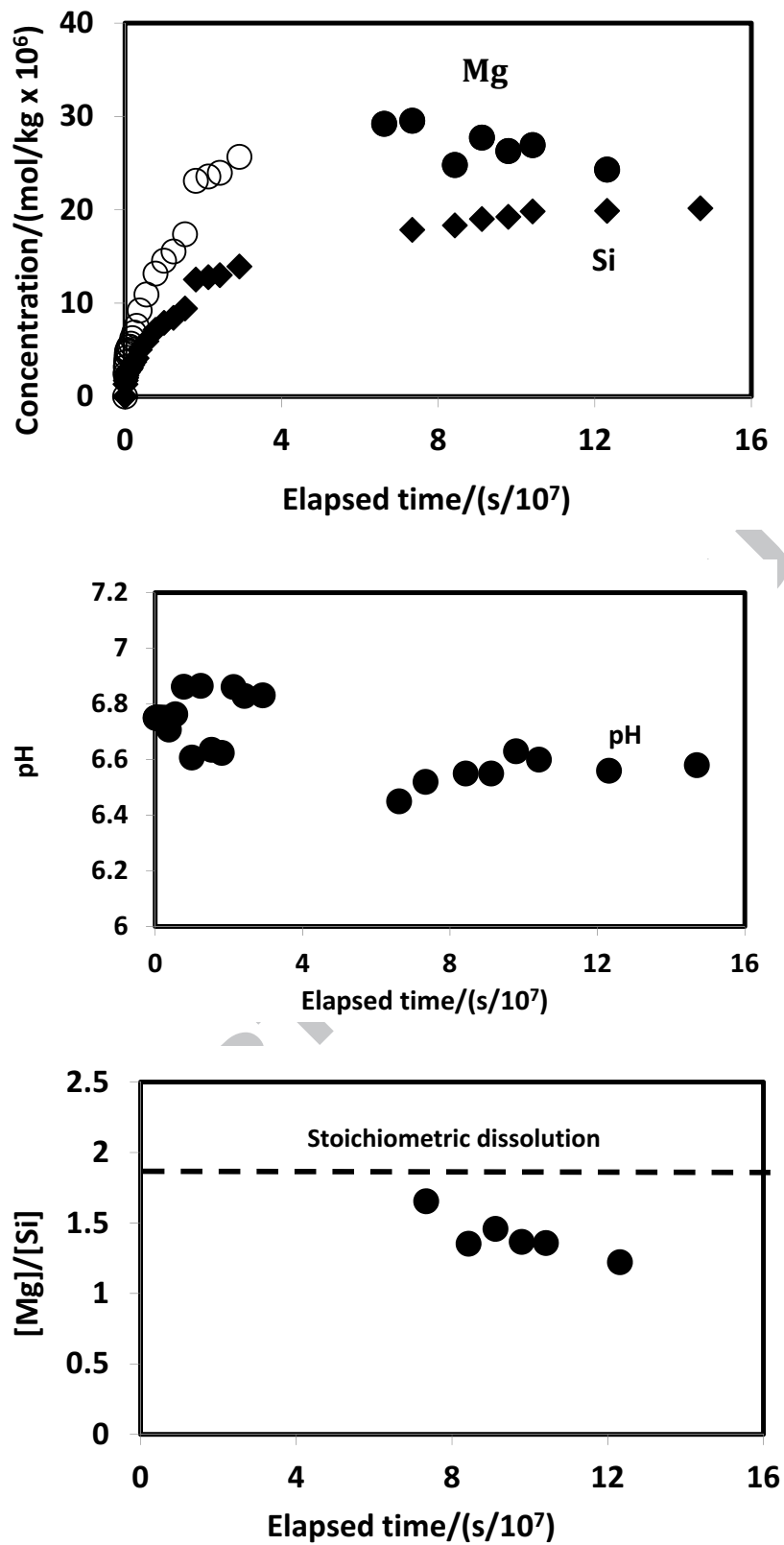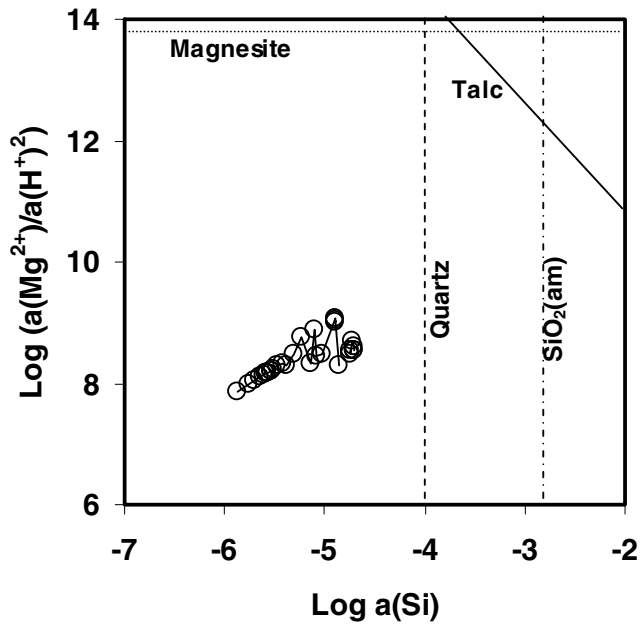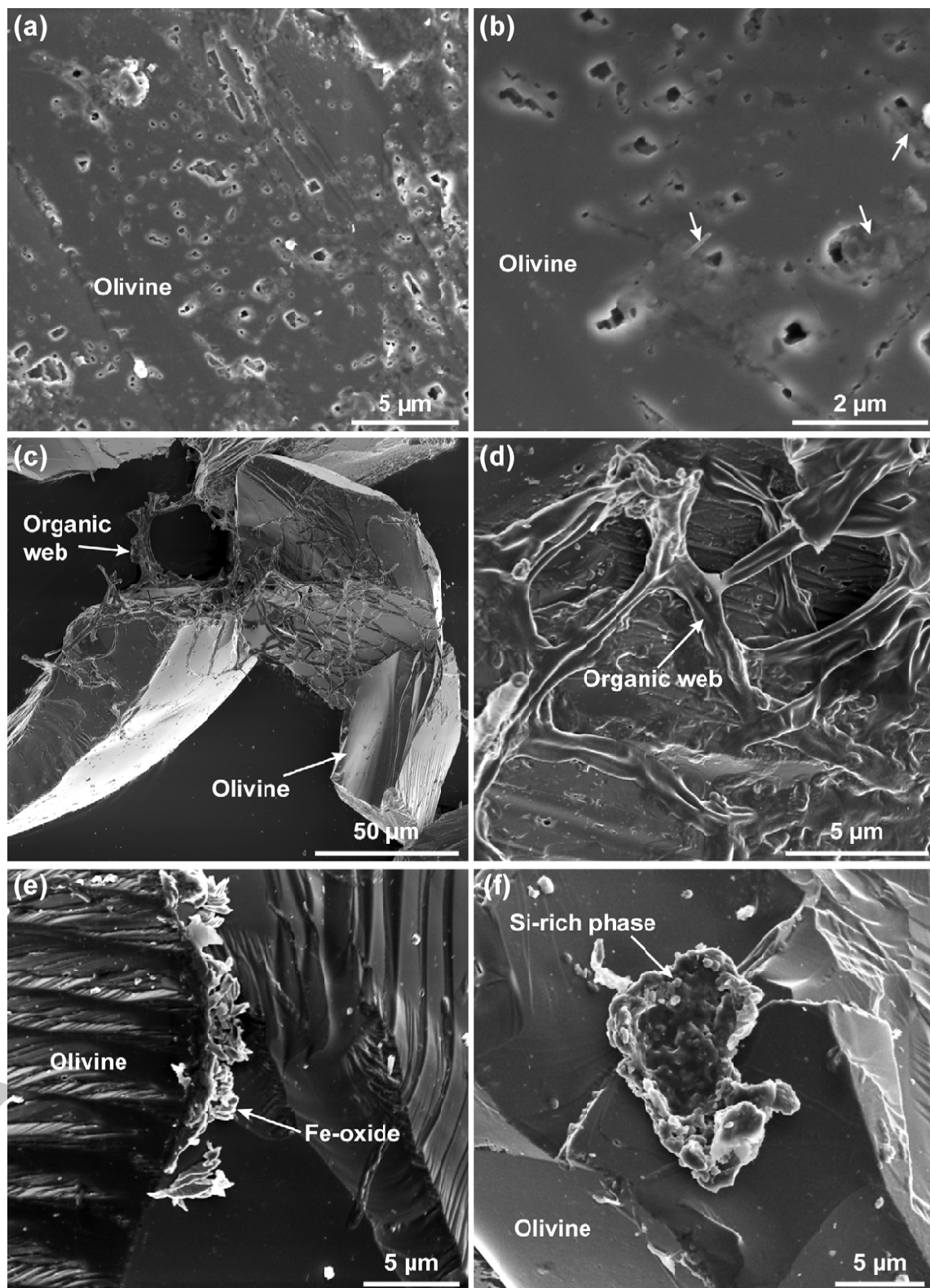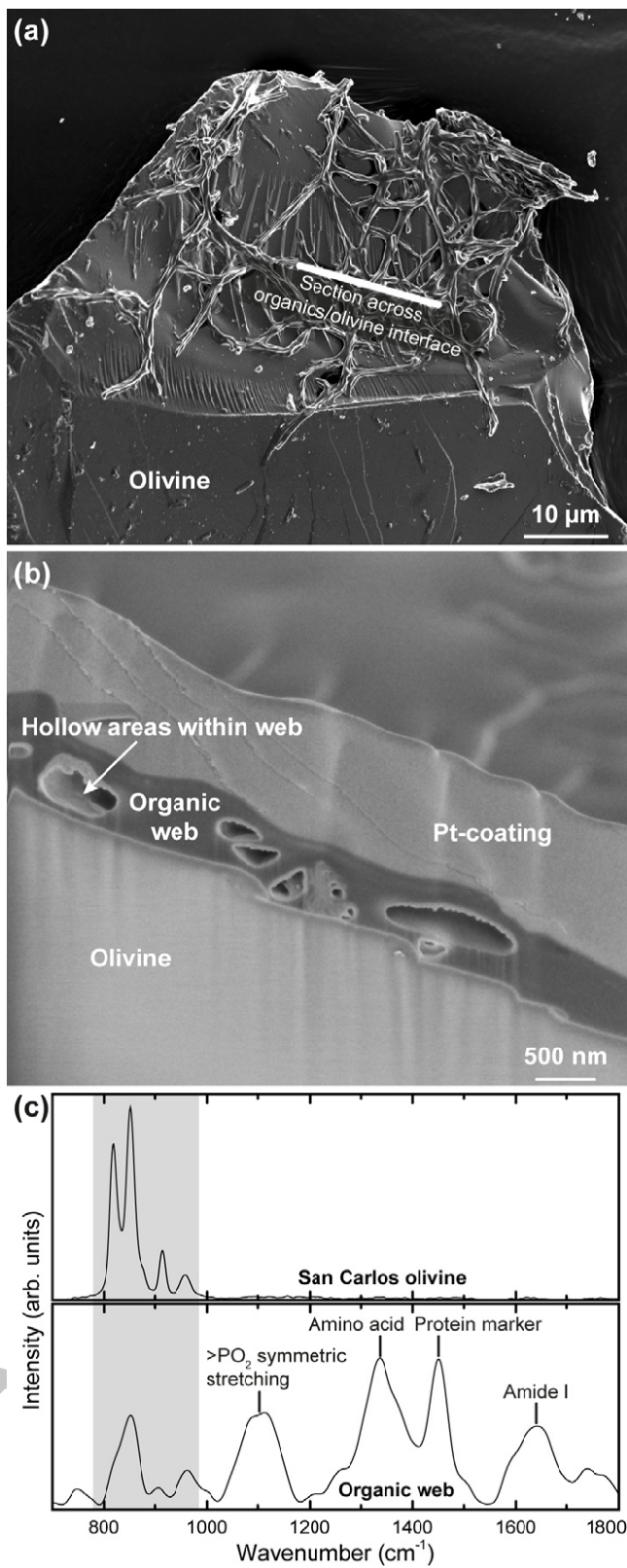
Figure 1

Figure 2

Figure 3.

Figure 4.

Figure 5.

Figure 6.

Figure 7.